Fast and simple tool for the quantification of biofilm-embedded cells sub-populations from fluorescent microscopic images

Short running title: tool for the quantitative analysis fluorescent images

Mikhail I Bogachev[1,2], Oleg A Markelov[1], Elena Trizna[2], Diana Baydamshina[2], Pavel Zelenikhin[2], Regina Murtazina[2], Airat R Kayumov[2,*]

[1]Biomedical Engineering Research Center, St. Petersburg Electrotechnical University, St. Petersburg, Russia

[2]Institute of Fundamental Medicine and Biology, Kazan Federal University, Russia

* Corresponding author

E-mail: kairatr@yandex.ru

Abstract

Fluorescent staining is a common tool for both quantitative and qualitative assessment of pro- and eukaryotic cells sub-population fractions by using microscopy and flow cytometry. However, direct cell counting by flow cytometry is often limited, for example when working with cells rigidly adhered either to each other or to external surfaces like in bacterial biofilms or adherent cell lines and tissue samples. An alternative approach is provided by using fluorescent microscopy and confocal laser scanning microscopy (CLSM), which enables the evaluation of fractions of cells subpopulations in a given sample. To facilitate the quantitative assessment of cell fractions in microphotographs, we suggest a simple two-step algorithm that combines the cell selection based and the statistical approaches. Based on a series of experimental measurements performed on bacterial and eukaryotic cells under various measurement conditions, we show explicitly that the suggested approach effectively accounts for the fractions of different cell sub-populations (like the live/dead staining in our samples) in all studied cases that are in good agreement with manual cell counting on microphotographs and flow cytometry data. This algorithm is implemented as a simple software tool that includes an intuitive and user-friendly graphical interface for the initial adjustment of algorithm parameters to the microscopic imaging conditions as well as for the sequential analysis of homogeneous series of similar microscopic images without further user intervention. The software tool entitled *BioFilmAnalyzer* is freely available online at http://kpfu.ru/eng/strau/laboratories/molecular-genetics-of-microorganisms-lab/software/ biofilmanalyzer-v10

Introduction

One of the key issues in both pro- and eukaryotic cell studies is the quantitative characterization of cellular subpopulations like the estimation of the fractions of either live or dead cells in a given population, differentiation of bacterial species in mixed biofilms or eukaryotic cell types in culture. There are two common experimental approaches to these issues, namely the flow cytometry and the fluorescent microscopy. In both methods the cells are stained with fluorescent dyes which specifically differentiate the cells of interest. Thus, Syto9/PI, DioC6/PI, AO/PI, CFDA/PI, Calcein AM/PI, Hoechst/PI and many other combinations of dual staining are widely used to differentiate viable and non-viable cells [1-3]. Normally, the first dye is biochemically modified by viable cells followed by the production of the green-fluorescent product. The second dye like the propidium iodide or ethidium bromide penetrates through the damaged membrane of dead cells forming complexes with nucleic acids and providing red fluorescence. While many researchers report that the estimation of viable cells fraction by using vital staining often exhibits significant differences in comparison with the values obtained by using classical microbiological methods [4], fluorescent staining remains a fast and easy approach to the quantification of (non-)viable cells.

While flow cytometry provides with a much more accurate assessment of the cell subpopulation fractions [5, 6], it has principal limitations that significantly narrow its application area [7]. In particular, cells being adhered to each other and to external surfaces should be suspended prior to their infusion into a cytometer that appears difficult when, for example, bacterial biofilms or strongly adherent cells are analyzed, or the original structure of the cell colonies, cell complex or tissue structure should be preserved. Moreover, flow cytometer is normally unable to detect particles <0.500 μm [8]. Finally, currently available flow cytometry systems require considerable amount of maintenance and highly skilled operators.

Fluorescent microscopy is largely free of above limitations and provides a reasonable

alternative to the cytometric measurements. However, in the presence of adherent and/or spore-like cells they largely overlap leading to the limitations of direct cell selection and counting algorithms in the microscopic images. The situation gets even more complicated when the cells are not equidistantly stained, image quality and color balance varies in different fields of view. Manual counting is usually possible, while it requires significant efforts from experts increasing the lab personnel workload drastically. Thus, automatic or semi-automatic analysis of cells seems to be a fast and easy approach for the microscopic data quantification. In the last two decades, a number of methods and computer-assisted algorithms have been developed to resolve the cell counting issue implemented in a number of both commercial and free software tools [9-13]. Existing software solutions include cell counting and classification algorithms [14], estimation of their parameters from microscopic imaging [15], 3d reconstructions from confocal microscopy data [16] and several other more specific applications. However, automatic microscopic image analysis remains challenging in the presence of adherent and/or spore-like cells that are common conditions in biofilm studies. Automatic counting methods are usually based either (i) on detection, selection and counting of discrete objects, or (ii) on the statistical analysis of the image properties that avoid direct counting approach and estimate some effective characteristics from the statistical properties of the entire image [17]. While the detection methods fail under cell overlapping conditions, the statistical assessment methods are unable to differentiate between various types of cells. Among few exceptions that largely overcome the above limitations, a very recently designed software tool for quantification of live/dead cells in a biofilm based on a series of image transformation could be mentioned [18].

Another common disadvantage of many automatic image analysis tools in practical settings is often, though may sound surprising, their excessive use of automation. Quite often image analysis algorithms use complex transformations with parameters that can be hardly controlled by a user who is not an expert in digital image processing. As a result, there is little or no feedback between the

95 algorithm and its end user. Thus, the user deals with a kind of black box design, where an image is
96 inserted and a value comes out, without being able to cross-check the performance of the algorithm at
97 some intermediate steps. Despite the increasing complexity and performance of image processing tools,
98 the variety of cell structures and microscopic imaging conditions to our opinion is still too broad to
99 fully rely upon automation in all cases.

100 Here we suggest an algorithm based on a simple combination of the object counting and
101 statistical approaches and easy-to-use cell-counting software tool, *BioFilmAnalyzer*, freely available at
102 http://kpfu.ru/eng/strau/laboratories/molecular-genetics-of-microorganisms-lab/software/
103 biofilmanalyzer-v10. Following preliminary threshold-based filtering and segmentation of the image,
104 an effective number of cells is calculated under partially-manual control by the investigator. Based on a
105 series of experimental measurements performed in bacterial cells of *S.auerus* and *B.subtillis* exhibiting
106 different shapes as well as eukaryotic cells, we show explicitly that the suggested approach effectively
107 account for the fractions of live/dead cells in all studied cases. The validity of the *BioFilmAnalyzer*
108 based cells live/dead fractions quantification was assessed by comparison with the results of manual
109 counting performed by several experts in visual microscopic image analysis and cytometric
110 measurements.

111

112

Materials and methods

Bacterial strains, cell lines and fluorescent microscopy

The fluorescent microscopic images of bacterial cells obtained in previous works were used [21, 22, 23, 24]. Briefly, *Staphylococcus aureus* (ATCC® 29213™) and *Bacillus subtilis 168* grown in 35-mm TC-treated polystyrol plates (Eppendorf) for 48 hours under static conditions at 37°C to obtain rigid biofilm structures were further subjected to differential live/dead fluorescent staining.

The human colon adenocarcinoma Caco-2 cells (RCCC) were cultured in DMEM supplemented with 10% FBS, 2 mM L-glutamine, 100 μg ml^{-1} penicillin and 100 μg ml^{-1} streptomycin. The cells were seeded in 24-well plates at the density of 30000 cells per well and allowed to attach overnight. The cells were cultured at 37 ºC and 5% CO_2 until 70% confluence and camptothecin (Sigma-Aldrich) was added in final concentration of 6 μM. After 24 h of exposition the cells were subjected to fluorescent staining and analyzed with flow cytometry and fluorescent microscopy.

The viability of biofilm-embedded cells was evaluated by staining for 5 min with the Acridine orange (Sigma) at final concentration of 0.12 μg/ml (green fluorescence) 3,3′-Dihexyloxacarbocyanine iodide (DioC6) (Sigma) at final concentration of 0.02 μg/ml (green fluorescence) and propidium iodide (Sigma) at final concentration of 3 μg/ml (red fluorescence) to differentiate between bacteria with intact and damaged cell membranes (live and dead cells). The eukaryotic cells were stained with DioC6 (0.02 μg/ml) and propidium iodide (3 μg/ml). The microscopic imaging was performed using either Carl Zeiss Observer 1.0 microscope or Carl Zeiss CLSM780 with 40-100× magnification.

Flow cytometry

Cytometric analysis was performed using BD FACSCanto II flow cytometer. The Caco-2 cells were stained as described above. Following data analysis was carried out using FACSDiva software.

Image analysis methodology

Image analysis starts with the preliminary detection of pixels with given color channel intensity (red, green or overall) exceeding a given threshold. Fig 1A shows a sample of original microscopic image, while Fig 1B shows the result of threshold-based selection of the red channel according to $I_R - I_G > T$, where I_R and I_G are the intensities in the red and in the green channels, respectively, $T = 30$ is the threshold setting. In the next step, the preprocessed image is segmented into separate non-overlapping objects by adjusting horizontally, vertically or diagonally neighboring pixels above the threshold to the same object. Additionally, objects with a given set of properties that determine the cell subpopulation are selected. Fig 1C exemplifies the results of selection by size, with objects only in a given size range between $s_{\min}$ = 500 and $s_{\max}$ = 1000 pixels being highlighted, where the color encodes each object.

In the following, we count the selected objects, calculate their total area, and obtain the average size of the typical cell from the studied subpopulation. Next we determine the effective number of cells by dividing the total area above the threshold (Fig 1B) by the average size of selected cells (Fig 1C) according to

$$N_R^{\text{eff}} = \frac{S_R}{\overline{S}_R\left[s_{\min} \ldots s_{\max}\right]} \text{ и } N_G^{\text{eff}} = \frac{S_G}{\overline{S}_G\left[s_{\min} \ldots s_{\max}\right]},$$

where N_R^{eff}, N_G^{eff} are the effective numbers of cells in the red and green channels, respectively; S_R, S_G are the total area of selected cells belonging to the red and green channels, respectively; $\overline{S}_R\left[s_{\min} \ldots s_{\max}\right]$, $\overline{S}_G\left[s_{\min} \ldots s_{\max}\right]$ are the average area of cells with a size range between $s_{\min}$ and

158 $s_{\max}$.

159

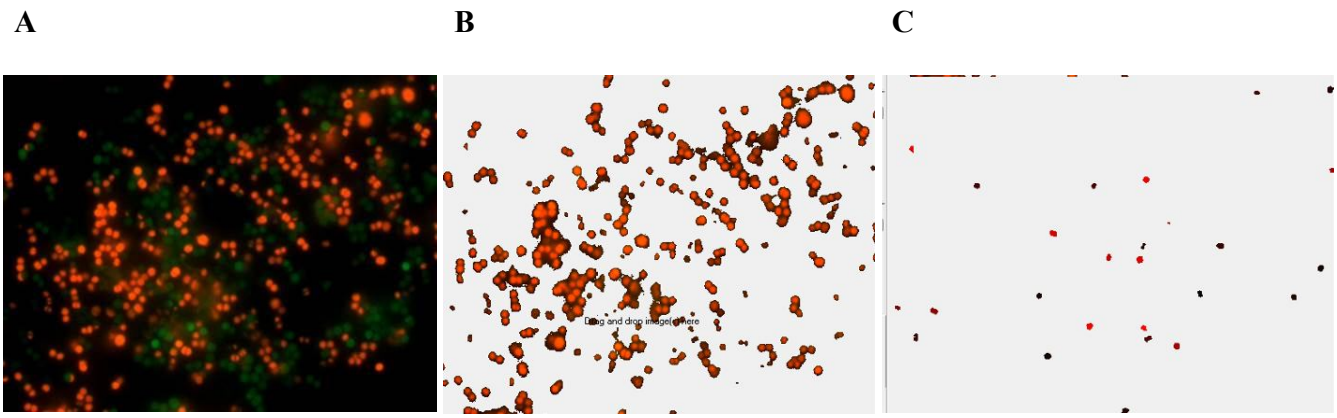

160 **Fig 1. Consecutive steps in cell quantification by *BioFilmAnalyzer*.** (A) original image containing
161 overlapped red and green channels, (B) selected red channel data after threshold-based filtering, (C)
162 selected cells of size between $s_{\min}$ and $s_{\max}$ that are used to determine the effective single cell size with
163 each separate cell shown by another color as determined by the automatic segmentation algorithm.

164

165 While T, $s_{\min}$ and $s_{\max}$ have to be appropriately chosen, their choice has to be performed once
166 in a series of similar experiments considering similar cell types. Accordingly, so far their manual choice
167 by expert seems to be the easiest solution option, since the feedback from the first samples being tested
168 allows for a more specific adjustment of these parameters, to avoid potentially bizzare results that may
169 arise in the case of their blind application with no feedback. In the following, for the entire series of
170 experiments the parameters are fixed and no further manual adjustment is required. Thus a series of
171 images representing different fields of view under identical conditions in simply passed through an
172 algorithm. When the differences in the conditions are minor and do not change significantly the
173 microscopic images, but influence only some of their parameters like the live/dead cell fractions, such
174 as testing antimicrobials with gradually changing concentrations, several series of images can be
175 submitted without further adjustment of the algorithm parameters. The implemented software solution

176 organizes the results of calculations in a table, that could be exported, and represent them in a graph.

177

178 ## Statistical assessment

179 Here we used simple linear regression without intercept term, i.e. $y = kx$. In the suggested
180 regression model the ideal case corresponds to k=1 or simply $y = x$ that would mean perfect agreement
181 between automatic and manual expert counting. The quality of the results is characterized by two
182 independent coefficients. The first one is the standard coefficient of determination R^2. $R^2 = 1 - \frac{SS_{res}}{SS_{tot}}$,
183 where SS_{tot} is the total sum of squares $SS_{tot} = \sum_i \left(f_i - \bar{y} \right)^2$ and SS_{res} is the residual sum of squares
184 $SS_{res} = \sum_i \left(y_i - f_i \right)^2$, here $\bar{y} = \frac{1}{n} \sum_{i=1}^{n} y_i$ is the mean value of all analyzed data points and f_i is
185 calculated regression point. The R^2 coefficient indicates how well the analyzed data set is replicated by
186 the regression model.

187

188 In this investigation it is also important how close is the regression model to the ideal case
189 $y = x$. Therefore we introduce a similarly designed metric of how well the model $y = kx$ is close to the
190 ideal counting line $y = x$ which is called L^2. Its definition is similar to R^2 besides the calculation is done
191 for regression points f_i. SS_{res} for L^2 is calculated as $SS_{res} = \sum_i \left(f_i - x_i \right)^2$, where x_i is the corresponding
192 abscissa value for the current f_i, and SS_{tot} is the same as in R^2. In ideal case when observational
193 regression line follows $y=x$, $L^2 = 1 - \frac{\sum_i \left(f_i - x_i \right)^2}{\sum_i \left(f_i - \bar{f} \right)^2} = 1 - \frac{0}{\sum_i \left(f_i - \bar{f} \right)^2} = 1$. Thus both R^2 and L^2

194 coefficients range from 0 to 1.

195

196

197

Results and Discussion

Software description

BioFilmAnalyzer software can be used to count any bacterial or eukaryotic fluorescent stained cells from two-dimensional microphotographs provided either as single images or as a series of images obtained under similar conditions such as quality and magnification (for example, several views of the same sample taken with fixed camera settings). This in-house algorithm was implemented in C++ programming language and is compatible with Windows (XP versions and higher). The software tool has a simple user-friendly environment for the image analysis with the two-step algorithm allowing manual parameter adjustments by end user at each step. The logic of the image analysis is based on the preliminary adjustment of the algorithm parameters by using one or several images that the investigator finds more or less representative for the studied cohort in terms of imaging conditions. In the first step, simple drag & drop of a single image into the program window initiates its instant processing including threshold based detection of cells according to a specified rule based on the exceedance of a given threshold by either a certain color channel, difference between color channels or overall intensity. The threshold value T which is the only algorithm parameter in this first step can next be adjusted by the investigator by its increasing in cases of strongly autofluorescent background or by its decreasing in low contrast images until the background noise is eliminated. For image series exhibiting strongly non-homogeneous color distributions in the studied color channels, instead of the manual adjustment of the threshold value T for each of the images individually, preliminary image color normalization often appears a faster alternative. Since color normalization is a simple and standard image preparation procedure that is straightforward and thus can be applied consecutively to a series of images using many commercial or free image processing software tools (e.g., ImageMagick, Gimp etc.), we do not focus further on this issue. However, as we show below, since our algorithm is robust against moderate variations of the threshold T around its optimized value for a given color distribution, the color

222 normalization appears unnecessary for image series with moderate variations of color distributions and
223 may be required only rarely under considerable variations of imaging conditions. The view can be
224 easily switched between the original and the processed images by a single click on the upper image
225 panel. In the second step, the effective cell size should be adjusted such that only or nearly only single
226 cells appear in the lower image panel, which shows the processed image after a simple segmentation
227 procedure. Increasing of the lower limit for the cell size helps to eliminate some noise bursts, while
228 increasing of the upper limit eliminates large patches of adherent cells from the effective cell size
229 statistics. With the cell size window representing only a simple criteria that often appears insufficient,
230 whenever necessary, further elimination of anomalous segments can be done manually by selecting and
231 double-clicking over them in the lower image panel. Since the parameters including sizes of different
232 sub-population of cells can differ from one another (e.g., non-viable eukaryotic cells are commonly
233 smaller than viable cells), the effective cell size should be re-adjusted for each studied sub-population
234 of cells. For this reason, the analysis of each color channel should be performed separately, and thus
235 with the exception of the intensity based analysis rule, all other options analyze color channels
236 individually. Thus they perform similarly for single or overlapped color channel images. Finally, the
237 effective number of cells is determined as the total area of the image exceeding the threshold T shown
238 in the upper panel divided by the effective cell size determined from the lower image panel. Once a
239 reasonable set of algorithm parameters in found, a series of up to 100 images can be dropped onto the
240 program window for fully automated analysis with the same set of parameters as determined from the
241 first one or several representative images without further user intervention. Finally, the results can be
242 exported to the MS Excel for the validation of the results and following statistical analysis.

243 In comparison with some other freely available image processing and analysis software [18-20],
244 our image-processing procedure is semi-automatic: settings are modified by manually adjusting the
245 analysis parameters and each step is controlled with an expert to evaluate the analysis quality. Being

246 optimized once for a first image in a series the software analyzes other images automatically over
247 coffee-break.

248 ## Software validation by bacterial cells counting

249 We analyzed the efficiency of the proposed algorithm using the fluorescent images of coccal
250 (*Staphylococcus aureus*) and rod (*Bacillus subtilis*) cell morphologies containing different fraction of
251 viable (green-stained) cells. Since the cell suspension can be easily analyzed with flow cytometry, we
252 focused on the analysis of adherent, biofilm-embedded cells. For that, we used previously obtained
253 series of microphotographs of *S.aureus* in 48-72 h old biofilms treated with different antimicrobials
254 [21, 22]. Cells were stained with DioC6 and propidium iodide to differentiate the viable and non-viable
255 cells, and non-viable cells fraction was quantified with *BioFilmAnalyzer* software. As a representative
256 example, twelve images with overlapped red and green channels containing different fraction of viable
257 cells are shown in Fig 2. Since the image brightness, contrast and saturation vary from image to image
258 depending on the staining quality, microscope settings and sample itself, for each microphotograph
259 shown in Fig 2 the thresholds T (ranging from 25 to 55) and effective cell sizes were chosen
260 individually. Next to validate the performance of the algorithm when the intensity threshold is chosen
261 quite arbitrarily without careful manual adjustment to the imaging conditions, these microphotographs
262 were analyzed consequently for different analysis thresholds (15, 20, 30, 45 and 60) and the results
263 obtained by the automatic cell counting were plotted as a linear function $y=kx$ of the manual cell
264 counting (Fig 3 A-C). While the number of both red (non-viable, Fig 3A) and green (viable, Fig 3B)
265 cells decreases at higher thresholds, their fractions (i.e., live/dead ratio) remained similar for each
266 threshold value exhibiting no significant differences with the manual evaluation data (compare thick
267 dashed line corresponding to the ideal fit of manual and automatic counting, Fig 3C).

268 Table 1 shows the regression coefficients k for the linear regressions $y=kx$ and their coefficients
269 of determination R^2. Since by definition there should be no systematic shift between the automatic and

the manual count, i.e. in the absence of viable or non-viable cells the respective number of cells equals zero, we used the simplest linear regression model without intercept. Since the ideal counting corresponds to k=1 or simply to the line given by $y=x$, we also calculated another coefficient denoted L^2 that determines the deviation of the obtained regression line $y=kx$ from the ideal counting line $y=x$. Of note, the automatic cell enumeration by *BioFilmAnalyzer* software exhibited the best fit with manual count at the analysis threshold of 45 (for images present on Fig 2). For further details on the statistical analysis of our results, we refer to the Materials and Methods section at the end of this paper.

The individual adjustment of the threshold and effective cell size is obviously possible only when a small number of images should be analyzed. For a more accurate quantification, a series of 10 or more images from the same sample normally should be analyzed. The *BioFilmAnalyzer* software allows analysis with constant settings of threshold and cell size of 2 and more images when they are dragged & dropped simultaneously onto the program window. To estimate the performance of the software when the images with different quality are analyzed without individual optimization of the intensity threshold, the series of 115 microphotographs randomly taken from different experiments were analyzed consequently at different thresholds (15, 20, 30, 45 and 60) with fixed cell size ranges used to determine the effective cell sizes. The results were compared against manual cell counting data (Fig 3 D-F). Similarly to previous results obtained for 12 images with accurate settings of both thresholds and cell sizes, the live/dead ratio remains almost similar for each threshold value and the obtained regression fit is in an excellent agreement with the manual cell counting data indicated by L^2 being very close to 1.0 at thresholds in the range of 15-30 (Table 1).

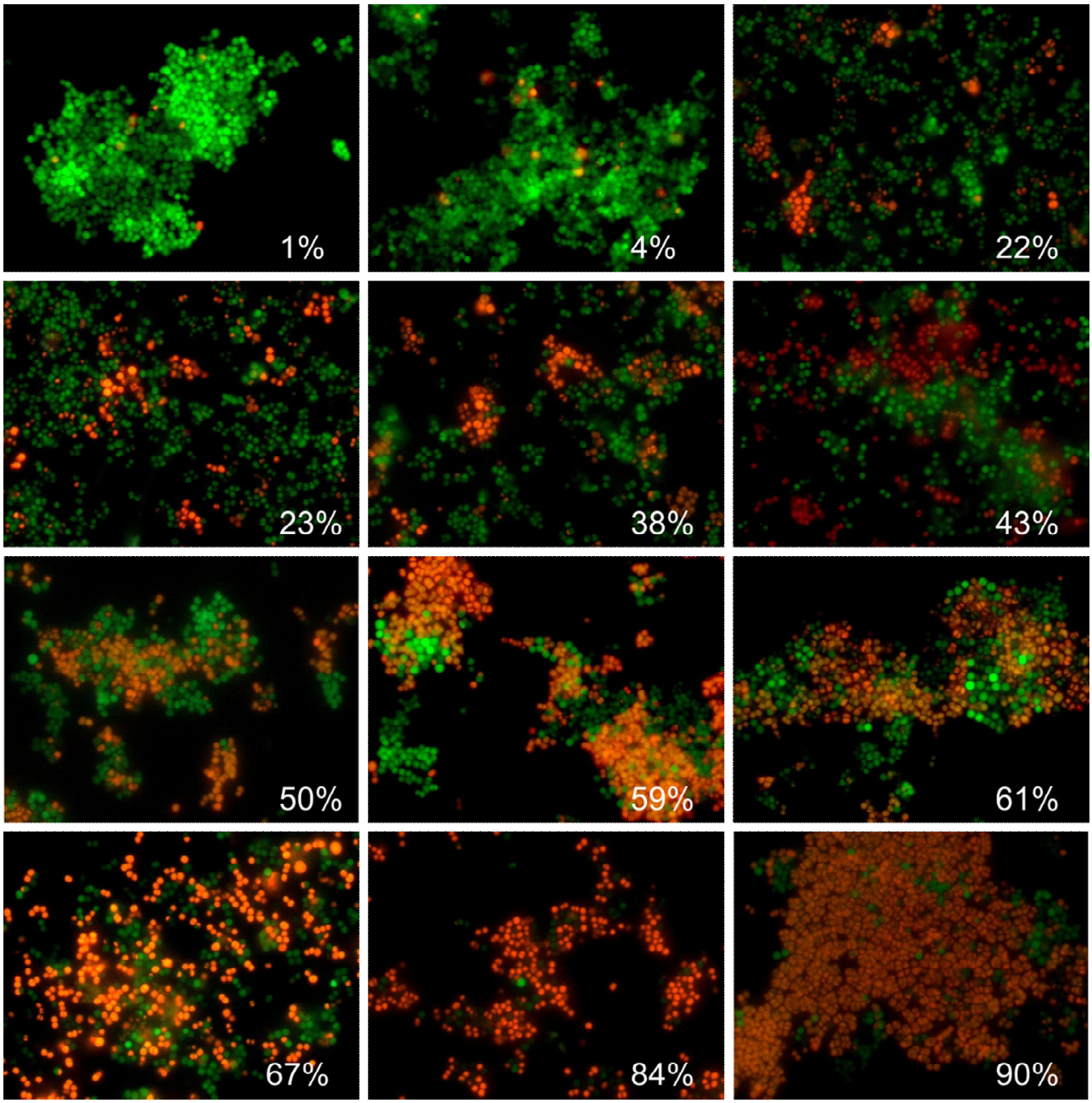

Fig 2. Evaluation of the *S.aureus* biofilm-embedded non-viable cells fraction by using *BioFilmAnalyzer* software exemplified for 12 microscopic images. The percentage of red-stained cells quantified by the *BioFilmAnalyzer* software is shown in each panel.

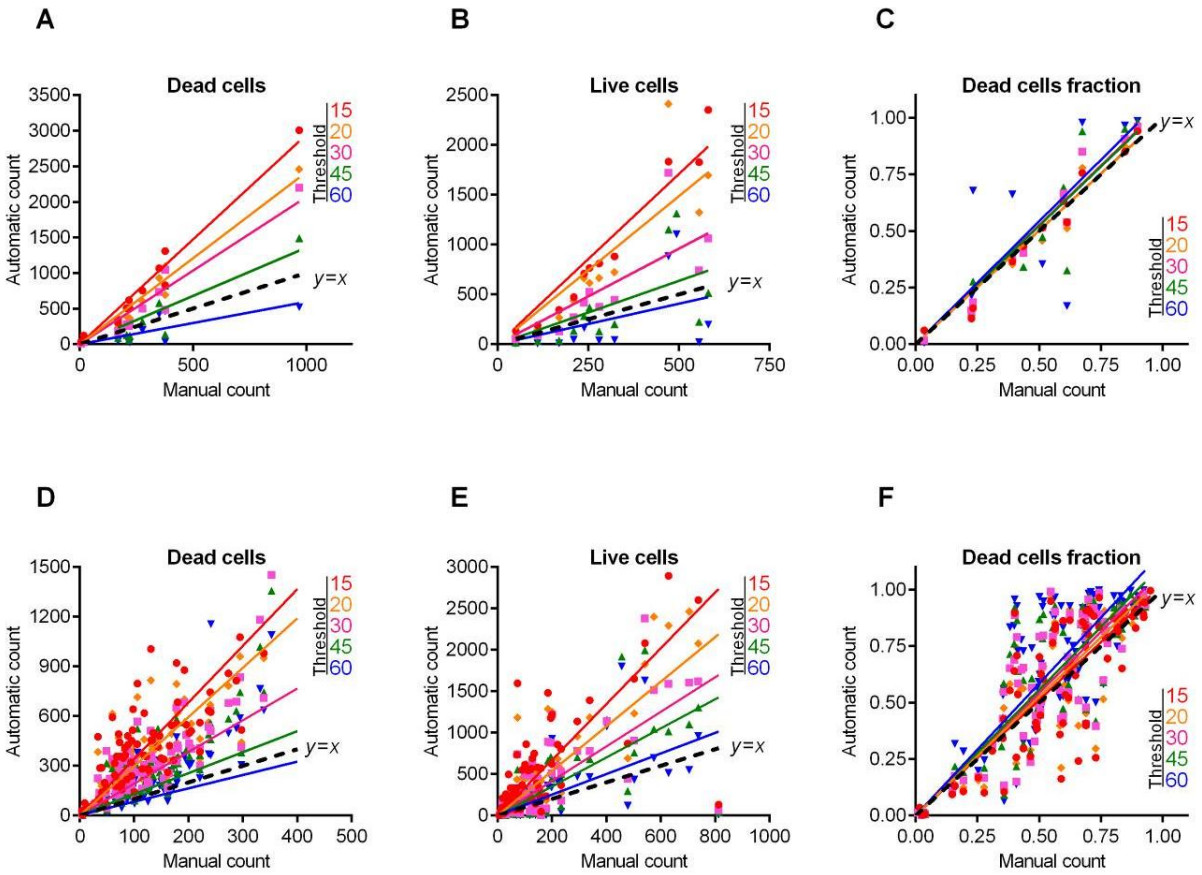

Fig 3. *S.aureus* cells count and live/dead ratio dependence on the image analysis threshold *T*. Full lines show the linear regression lines, while dashed line shows the ideal counting line as determined by the manual analysis performed by several experts in visual microscopic image analysis. Panels A-C show data for the 12 images presented in Fig 2. Panels D-F show data for the 115 microscopic images taken randomly from different experiments with various imaging conditions.

305 **Table 1. Regression coefficients *k*, the coefficients of determination R^2 and the accuracy**
306 **coefficient L^2 indicating the correspondence between the automatic and the manual counting for**
307 **the *S.aureus* live/dead ratios on fluorescent images.**

	12 images			115 images		
Threshold	k	R^2	L^2	k	R^2	L^2
15	1,01	0,95	1,00	1,02	0,63	1,00
20	1,00	0,94	1,00	1,05	0,65	0,99
30	1,05	0,94	0,99	1,08	0,66	0,98
45	1,05	0,73	0,99	1,11	0,72	0,96
60	1,09	0,59	0,98	1,17	0,67	0,92

308

309

Next, similar analysis was performed on microscopic images of *B.subtilis* biofilm-embedded cells treated with different antimicrobials [23]. Like in the previous example, Fig 4 shows 12 representative images with different fraction of viable cells quantified with *BioFilmAnalyzer* software. Fig 5 A-C is designed similar as Fig 3 and shows the interdependence of the image analysis threshold and cell number calculated by *BioFilmAnalyzer*. Similar to *S.aureus* microphotographs, the cell number calculated automatically increased at high threshold with the best fit with manual count at threshold value of 45, while the live/dead ratio remained unchanged with L^2 exceeding 0.96 at thresholds up to 45, suggesting that the performance of the algorithm does not depend on the fine tuning of the threshold and on the cell shape. Fig 5 D-F shows the analysis of 50 randomly chosen images of live/dead stained *B.subtilis* cells. Similarly, the statistical analysis does not reveal significant differences between automatic and manual live/dead ratio estimation (Table 2).

While the absolute cell counting depends on the image analysis threshold which should be adjusted manually and therefore has a factor of subjectivity, the live/dead ration quantification does not depend on the threshold settings in range of 15-60 color intensity units (on the 0..255 scale) exhibiting linear function with R^2 values exceeding 0.9 and regression coefficients of k ranging between 0.9 and 1.1 (Tables 1 and 2). This fact allows performing the automatic analysis of multiple images with constant settings optimized for first image in a series.

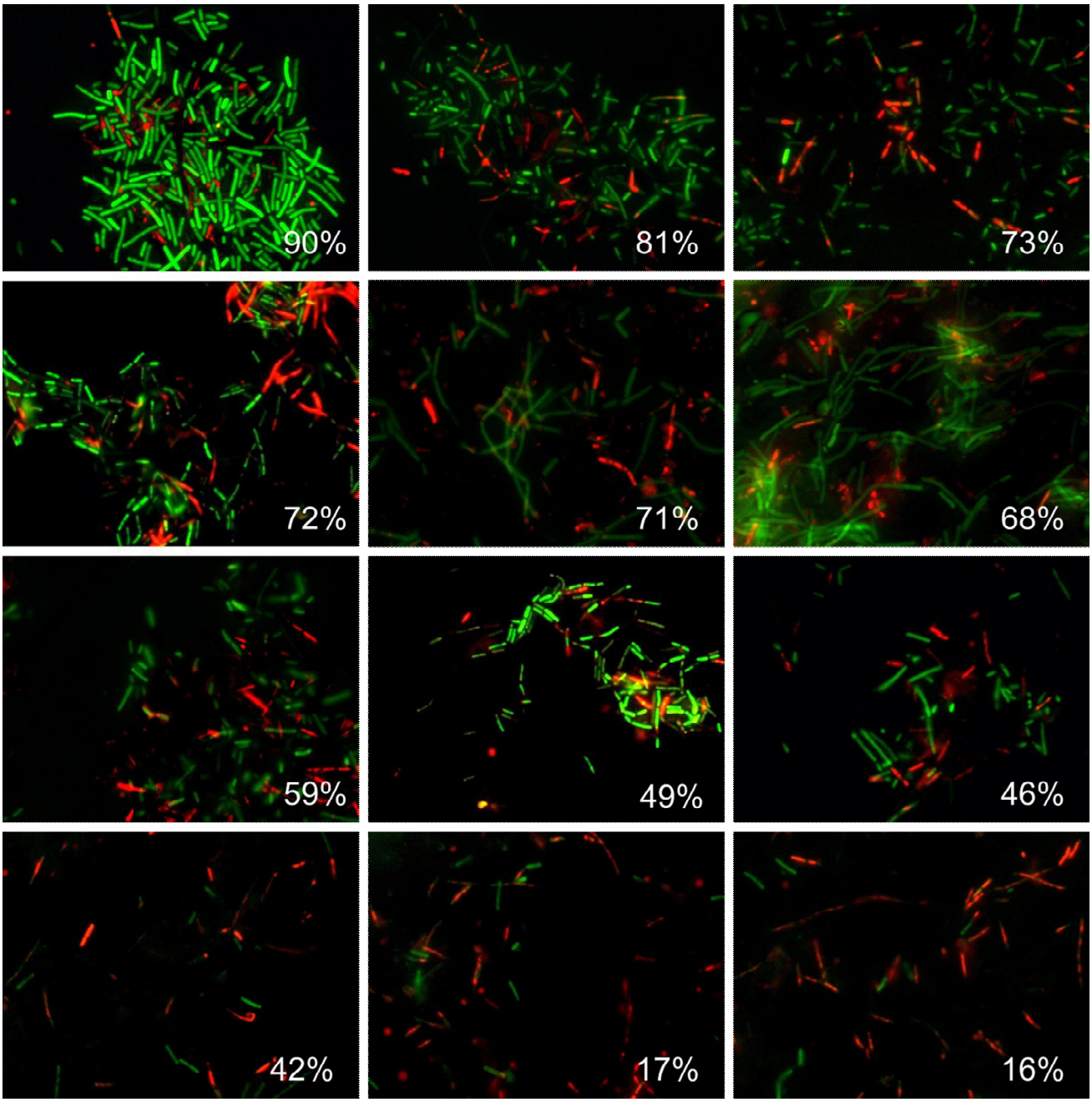

Fig 4. Evaluation of the *B.subtilis* biofilm-embedded non-viable cells fraction by using *BioFilmAnalyzer* software exemplified for 12 microscopic images. The percentage of red-stained cells quantified by the *BioFilmAnalyzer* software is shown in each panel.

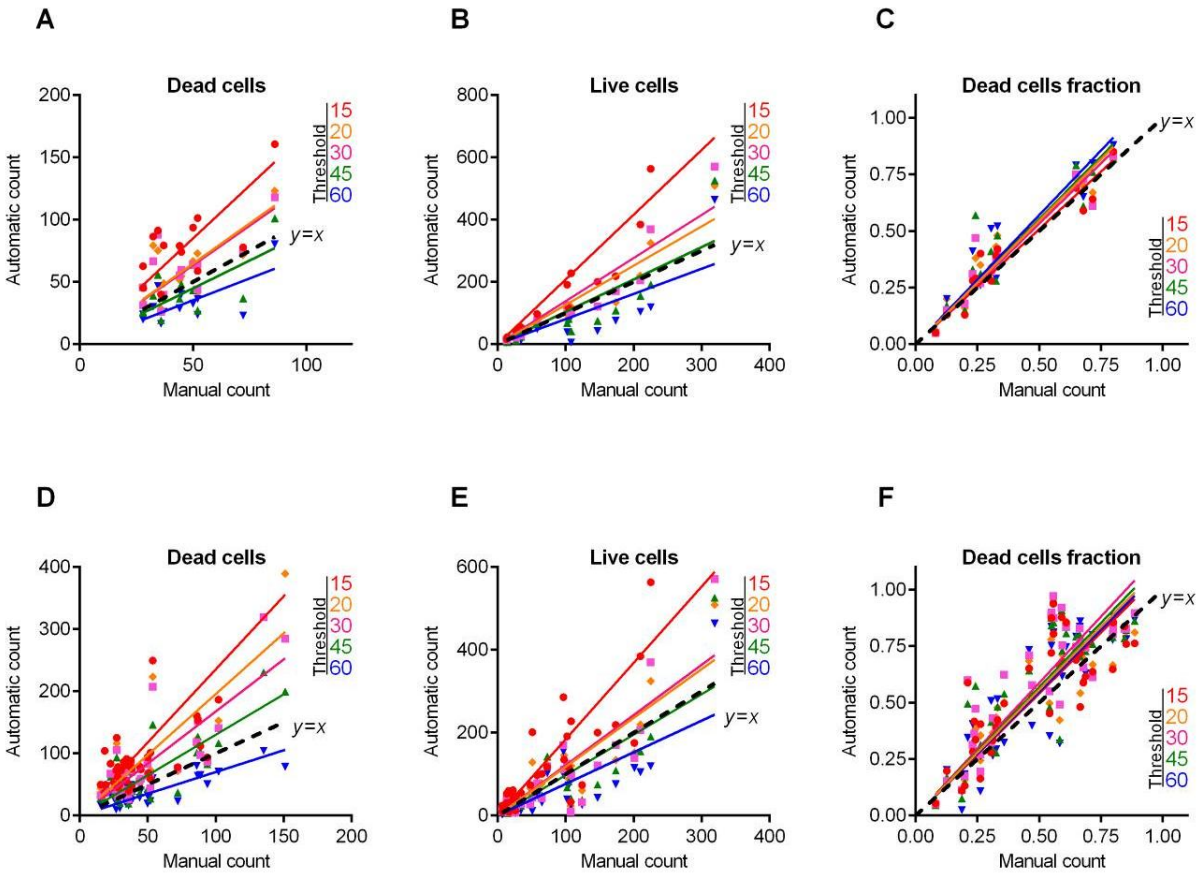

Fig 5. *B.subtilis* cells count and live/dead ratio dependence on the image analysis threshold *T*. Full lines show the linear regression lines, while dashed line shows the ideal counting line as determined by the manual analysis performed by several experts in visual microscopic image analysis. Panels A-C show data for the 12 images presented in Fig 4. Panels D-F show data for the 50 microscopic images taken randomly from different experiments with various imaging conditions.

Table 2. Regression coefficients *k*, the coefficients of determination R^2 and the accuracy coefficient L^2 indicating the correspondence between the automatic and the manual counting for the *B.subtilis* live/dead ratios on fluorescent images

	12 images			50 images		
Threshold	k	R^2	L^2	k	R^2	L^2
15	1,02	0,92	1,00	1,08	0,72	0,97
20	1,09	0,93	0,97	1,11	0,74	0,95
30	1,07	0,91	0,98	1,17	0,75	0,90
45	1,10	0,84	0,96	1,14	0,74	0,93
60	1,14	0,90	0,93	1,10	0,74	0,96

Eukaryotic cells counting

The performance of the *BioFilmAnalyzer* software was also analyzed for the eukaryotic cells. For that, Caco-2 cells were treated with different concentrations of camptothecin and analyzed after 24h of exposition. Fig 6 and 7C show the fractions of viable cells quantified with *BioFilmAnalyzer* software on microphotographs with overlapped green and red channels. Here, the best fit of manual and automatic count of either live or dead cells was observed with the analysis threshold T=30 (Fig 7), while higher background level led to artificial results at T=15 (not shown). In contrast to bacterial cells, the accuracy was lower (L^2 over 0.80), probably, because of discrepancies in cell sizes and non-evenly staining of cells. In contrast, when the software performance was evaluated on a series of 87 randomly chosen images (Fig 7 D-F), the automatic estimation of live/dead fractions fits with manual one with high confidence level (L^2 equals 1.0, see Table 3). This effect could be attributed to the larger effective sizes and thus also smaller average number of cells in each field of view for eukaryotic cells compared to bacterial cells that in turn requires analyzing more images in order to obtain similar statistics.

359

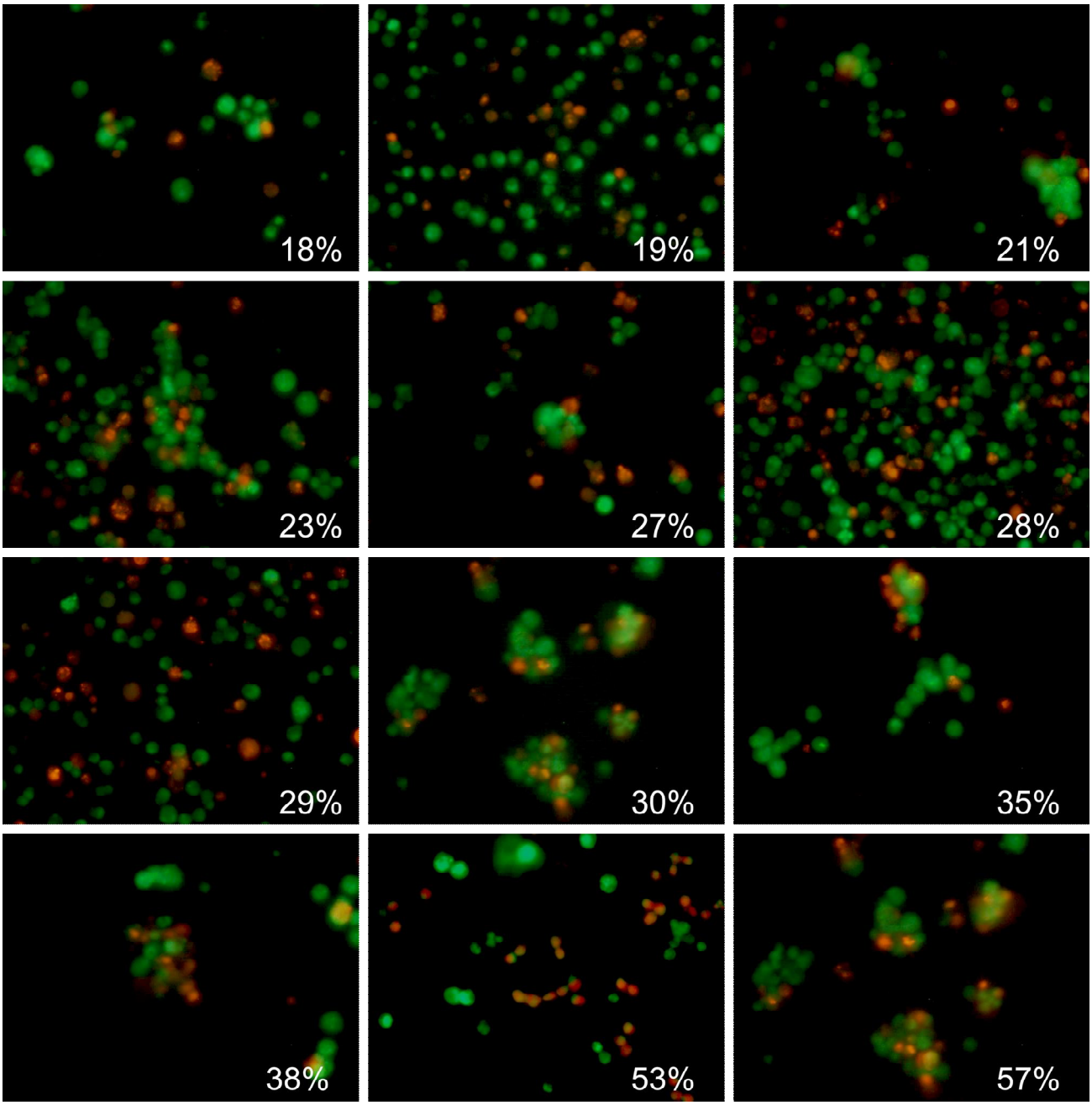

360

361 **Fig 6. Evaluation of the Caco-2 non-viable cells fraction by using *BioFilmAnalyzer* software**
362 **exemplified for 12 microscopic images.** The percentage of red-stained cells quantified by the
363 *BioFilmAnalyzer* software is shown in each panel

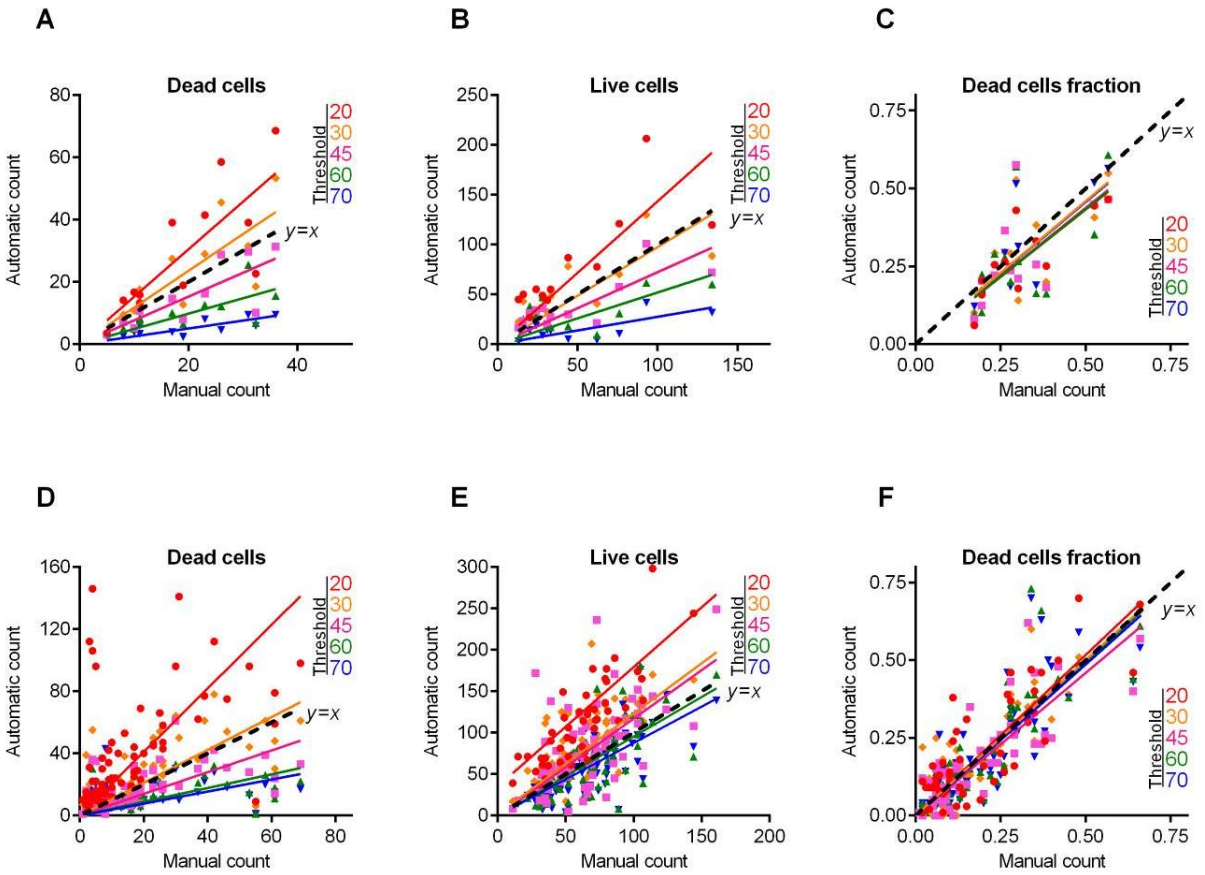

Fig 7. Caco-2 cells count and live/dead ratio dependence on the image analysis threshold *T*. Full lines show the linear regression lines, while dashed line shows the ideal counting line as determined by the manual analysis performed by several experts in visual microscopic image analysis. Panels A-C show data for the 12 images presented in Fig 6. Panels D-F show data for the 87 microscopic images taken randomly from different experiments with various imaging conditions

373 **Table 3. Regression coefficients *k*, the coefficients of determination R^2 and the accuracy**
374 **coefficient L^2 indicating the correspondence between the automatic and the manual counting for**
375 **the Caco-2 live/dead ratios on fluorescent images**

	12 images			87 images		
Threshold	k	R^2	L^2	k	R^2	L^2
15	nd	nd	nd	nd	nd	nd
20	0,86	0,69	0,80	1,03	0,73	1,00
30	0,92	0,53	0,93	1,00	0,76	1,00
45	0,88	0,46	0,83	0,92	0,71	0,97
60	0,87	0,40	0,81	0,99	0,73	1,00
70	0,91	0,54	0,92	0,97	0,71	1,00

376

377 To verify the accuracy of the overall procedure including the microscopy and automatic cells
378 counting, the treated cells were detached from the wells by trypsin treatment, stained with DioC6 and
379 ethidium bromide and aliquoted. One half of the sample was analyzed with flow cytometry to evaluate
380 the fraction of necrotic cells, while the other half was subjected to microscopy and quantified by
381 *BioFilmAnalyzer*. Fig 8 shows fractions of the non-viable cells in 4 independent repeats quantified with
382 flow cytometry versus automatic analysis of series of 10 microphotographs from each sample with
383 separate green and red channels (representative examples of images are shown in the figure).

384

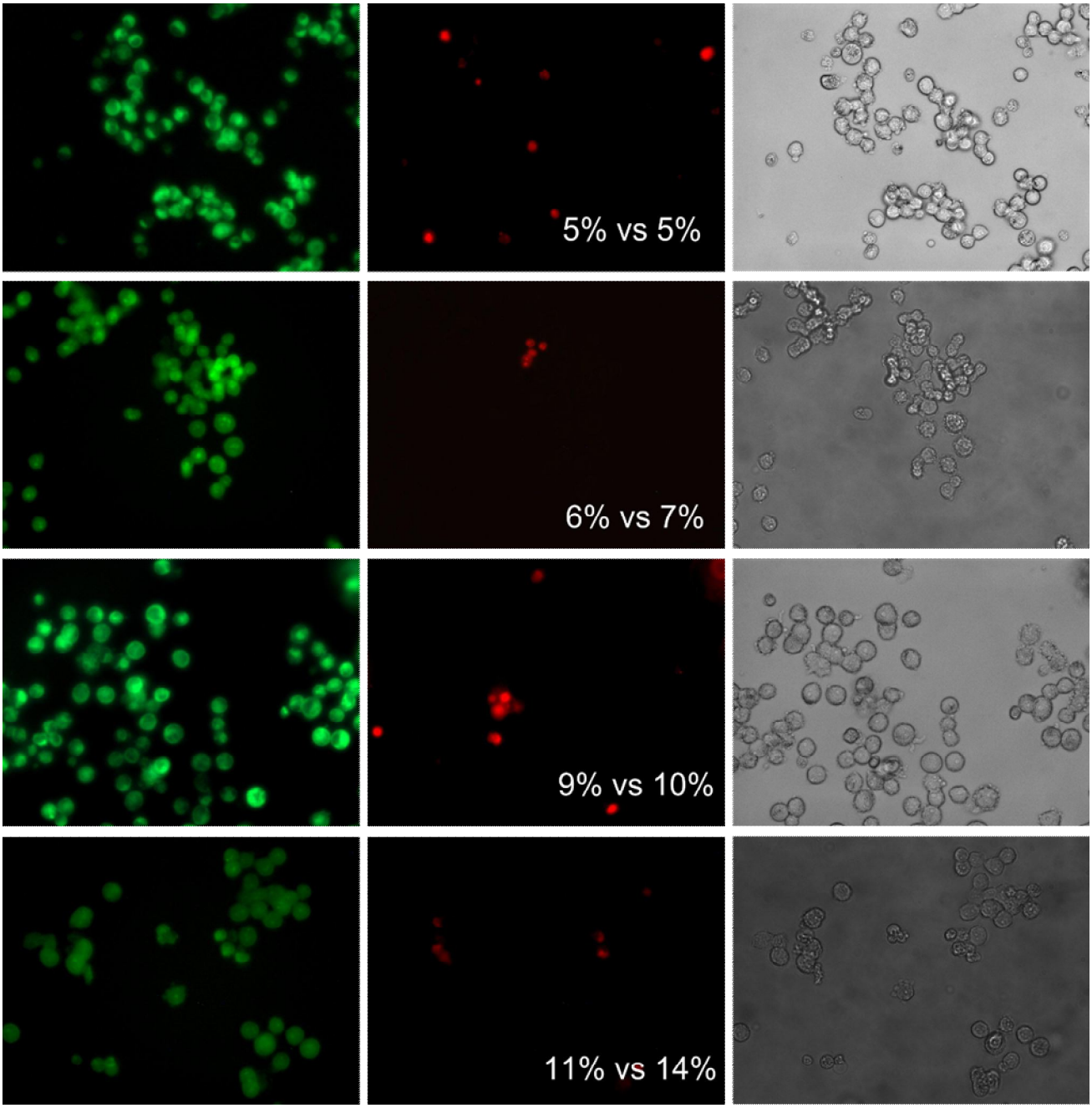

385

386 **Fig 8. The fraction of the non-viable eukaryotic cells quantified by flow cytometry versus**

387 **automatic analysis with *BioFilmAnalyzer*.**

388

Quantification of confocal images with Z-stacks

Finally, we used the same algorithm and software to analyze the confocal images with Z-stacks, including 4 confocal images of *S.aureus* cells treated with different antimicrobials from our recent work [24]. For that, we analyzed the raw series of 2D images that were used previously to reconstruct 3D images in [24], where the fraction of live/dead cells were evaluated by both automatic and manual expert counting (Fig 9).

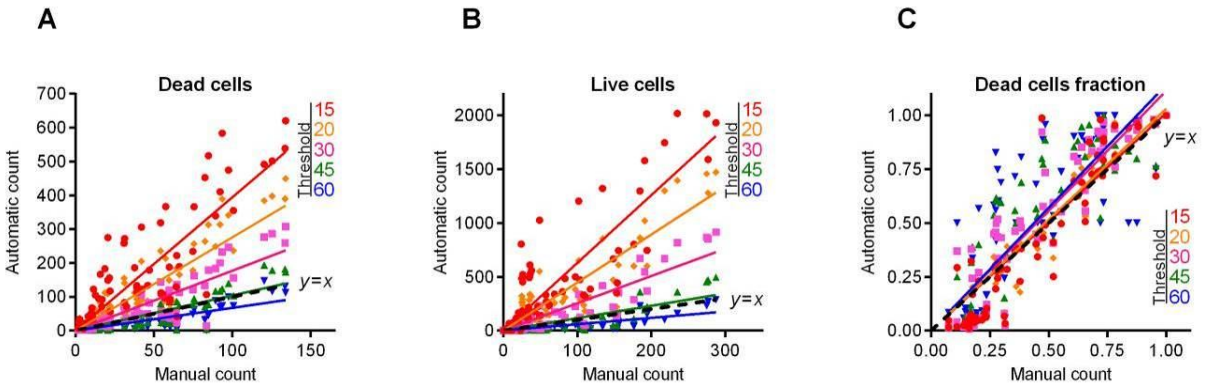

Fig 9. Automatic vs manual cell count cell count and live/dead ratio dependence for different image analysis thresholds *T*. Full lines show the linear regression lines, while dashed line shows the ideal counting line as determined by the manual analysis performed by several experts in visual microscopic image analysis. Four different confocal images containing between 12 and 23 Z-stacks each were taken for the analysis.

Typically 2d images obtained by confocal layer scanning technique are lower quality in comparison with single layer fluorescent microscopic images considered above. There are generally several contributing effects including defocus aberration of the cells that appear close but nevertheless displaced against the focal point due to the limited depth of focus as well as motion blur due to the

sample shift during operation. Both effects lead to blurred images, the problem that is partially resolved in the 3d reconstruction algorithms by averaging or smoothening filters that improve the overall image quality at the cost of its effective resolution. The question is, whether raw 2d images obtained by confocal layer scanning technique can be used for the cell sub-population quantification using our algorithm, and whether this would require some preliminary filtering to reduce blurring effects. For the latter, two standard image filtering techniques, namely the Gaussian and the Sobel filters have been tested. The Sobel filtering aims on edge detection in the images using a discrete differentiation operator which computes an approximation of the gradient of the image intensity function. Therefore this kind of image preparation might be helpful to make edges of cells more stepwise and thus to reduce the dependence of the performance of the cell counting algorithm on the choice of the threshold that may then appear anywhere within this step. Alternatively, blurring may be treated as effective additive noise that could be reduced with simple Gaussian filter. Exhibiting a Gaussian impulse response, such filter decreases the overall noise level in the image.

Figure 10 shows an example of the 2d confocal Z-stack microscopic image before and after Gaussian and Sobel filtering (upper panel) and the regression functions of automatic cells count at different thresholds as a function of the manual cell count (lower panel) before and after preliminary filtering of the images (obtained for the entire cohort of studied confocal images). The figure shows that, while the image appears visually less blurred, there is no significant improvement on cells fraction count according to the regression analysis results (see also Table 4). Furthermore, preliminary filtering leads to the overestimation of the red-stained cell count in some samples analyzed this way also corrupting the overall sub-population fraction estimates. Therefore, we find that due to the general robustness of the sub-population fraction estimation against the variations of the threshold T (and thus also its relation with the quantile of the image color distribution), 2d images obtained by confocal layer scanning technique can be analyzed without preliminary image filtering.

Table 4. Regression coefficients *k*, the coefficients of determination R^2 and the accuracy coefficient L^2 indicating the correspondence between the automatic and the manual counting for the *S.aureus* live/dead ratios on confocal images.

	No filters			Gaussian			Sobel		
Threshold	k	R^2	L^2	k	R^2	L^2	k	R^2	L^2
15	1,01	0,81	1,00	1,02	0,85	1,00	1,08	0,87	0,98
20	1,03	0,81	1,00	1,04	0,83	0,99	1,10	0,84	0,97
30	1,11	0,82	0,95	1,15	0,76	0,92	1,17	0,77	0,92
45	1,14	0,77	0,93	1,25	0,71	0,78	1,24	0,79	0,87
60	1,14	0,68	0,93	1,32	0,60	0,69	1,30	0,78	0,78

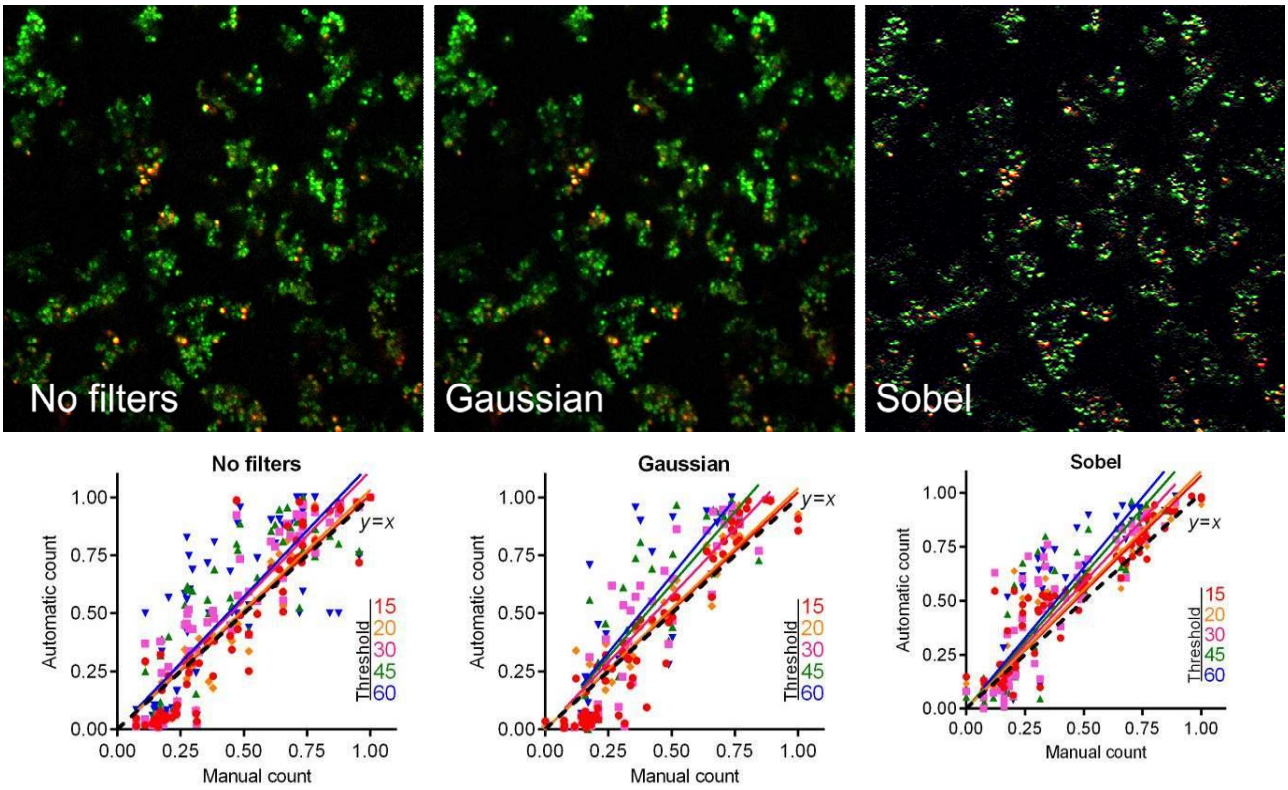

Fig 10. The live/dead ratio dependencies for different image analysis thresholds *T*. Full lines show the linear regression lines, while dashed line shows the ideal counting line as determined by the manual analysis performed by several experts in visual microscopic image analysis. Four confocal images containing between 12 and 23 Z-stacks were taken for the analysis, before and after being subjected to either Gaussian or Sobel filtering, as indicated.

Conclusion

To summarize, our results indicate that the sub-population fraction estimates obtained from fluorescent-stained cells imaging data by *BioFilmAnalyzer* are very close to the results obtained by other techniques such as expert manual counting and flow cytometry. The two-step algorithm implemented in the *BioFilmAnalyzer* that normalizes the stained image area in the units of the effective single cell size that are determined under partial manual control by the investigator performs largely independently of the cell shape and imaging conditions providing feasible results for cells aggregated in clusters. Moreover, in most cases no preliminary preparation or filtering of raw images is required.

Thus, we suggest that the proposed algorithm implemented as the *BioFilmAnalyzer* software can be used for numerous applications. First, preliminary evaluation of cell counts and live/dead ratios can be quickly obtained without expertise in image processing. Second, the analysis of surface-adherent bacterial or eukaryotic cells without their resuspension and maintenance of the native distribution pattern on the surface is possible. Third, the quantification of cellular sub-populations from 2d confocal layer images is also possible. Fourth, the software allows quantification of the cells sub-populations expressing fluorescent proteins in during long-time incubation. Finally, because no further user intervention is required after few initial adjustment and cross-check procedures which usually take a couple of minutes using few representative images, further processing can be done over coffee-break by automated analysis of a series of images.

We believe that the suggested algorithm and software would be useful in saving time and efforts in cells sub-population quantification from fluorescent microscopy data that is commonly required in various biomedical, biotechnological and pharmacological studies, especially for the analysis of biofilm-embedded cells where the performance of conventional techniques based on cell counting or flow cytometry is strongly limited. Both the algorithm and the *BioFilmAnalyzer* can be freely

471 downloaded at http://kpfu.ru/eng/strau/laboratories/molecular-genetics-of-microorganisms-
472 lab/software/biofilmanalyzer-v10, utilized and redistributed.
473
474

475 Acknowledgments

476 The financial support of this work was provided by the Russian Science Foundation (project
477 No. 15-14-00046, AK), by the Ministry of Education and Science of the Russian Federation (St.
478 Petersburg Electrotechnical University, assignment 2.5475.2017/6.7, MB) and by the Program of
479 competitive development of Kazan Federal University. The funders had no role in study design, data
480 collection and analysis, decision to publish, or preparation of the manuscript.
481

482 **Data Availability:** All data are within the manuscript. The algorithm proposed in this
483 manuscript is implemented as a simple software tool entitled *BioFilmAnalyzer* is freely available online
484 at http://kpfu.ru/eng/strau/laboratories/molecular-genetics-of-microorganisms-
485 lab/software/biofilmanalyzer-v10
486
487

References

1. Tawakoli PN, Al-Ahmad A, Hoth-Hannig W, Hannig M, Hannig C. Comparison of different live/dead stainings for detection and quantification of adherent microorganisms in the initial oral biofilm. Clinical Oral Investigations. 2013;17(3):841-50. doi: 10.1007/s00784-012-0792-3. PubMed PMID: WOS:000316749300019.

2. McMullan BJ, Desmarini D, Djordjevic JT, Chen SCA, Roper M, Sorrell TC. Rapid Microscopy and Use of Vital Dyes: Potential to Determine Viability of Cryptococcus neoformans in the Clinical Laboratory. Plos One. 2015;10(1). doi: 10.1371/journal.pone.0117186. PubMed PMID: WOS:000348821400028.

3. Atale N, Gupta S, Yadav UCS, Rani V. Cell-death assessment by fluorescent and nonfluorescent cytosolic and nuclear staining techniques. Journal of Microscopy. 2014;255(1):7-19. doi: 10.1111/jmi.12133. PubMed PMID: WOS:000339710500002.

4. Netuschil L, Auschill TM, Sculean A, Arweiler NB. Confusion over live/dead stainings for the detection of vital microorganisms in oral biofilms - which stain is suitable? Bmc Oral Health. 2014;14. doi: 10.1186/1472-6831-14-2. PubMed PMID: WOS:000330071900001.

5. Gerstner AOH, Mittag A, Laffers W, Dahnert I, Lenz D, Bootz F, et al. Comparison of immunophenotyping by slide-based cytometry and by flow cytometry. Journal of Immunological Methods. 2006;311(1-2):130-8. doi: 10.1016/j.jim.2006.01.012. PubMed PMID: WOS:000237527200013.

6. Mital J, Schwarz J, Taatjes DJ, Ward GE. Laser scanning cytometer-based assays for measuring host cell attachment and invasion by the human pathogen Toxoplasma gondii. Cytometry Part A. 2006;69A(1):13-9. doi: 10.1002/cyto.a.20202. PubMed PMID: WOS:000234383700002.

7. Adan A, Alizada G, Kiraz Y, Baran Y, Nalbant A. Flow cytometry: basic principles and applications. Critical Reviews in Biotechnology. 2017;37(2):163-76. doi: 10.3109/07388551.2015.1128876. PubMed PMID: WOS:000392639500003.

8. van der Pol E, Hoekstra AG, Sturk A, Otto C, van Leeuwen TG, Nieuwland R. Optical and non-optical methods for detection and characterization of microparticles and exosomes. Journal of Thrombosis and Haemostasis. 2010;8(12):2596-607. doi: 10.1111/j.1538-7836.2010.04074.x. PubMed PMID: WOS:000285110700003.

9. Heydorn A, Nielsen AT, Hentzer M, Sternberg C, Givskov M, Ersboll BK, et al. Quantification of biofilm structures by the novel computer program COMSTAT. Microbiology-Sgm. 2000;146:2395-407. PubMed PMID: WOS:000089985400007.

10. Beyenal H, Donovan C, Lewandowski Z, Harkin G. Three-dimensional biofilm structure quantification. Journal of Microbiological Methods. 2004;59(3):395-413. doi: 10.1016/j.mimet.2004.08.003. PubMed PMID: WOS:000224843300009.

11. Merritt JH, Kadouri DE, O'Toole GA. Growing and analyzing static biofilms. Curr Protoc Microbiol. 2005;Chapter 1:Unit 1B. doi: 10.1002/9780471729259.mc01b01s00. PubMed PMID: 18770545; PubMed Central PMCID: PMCPMC4568995.

12. Ji L, Piper J, Tang JY. Erosion and dilation of binary images by arbitrary structuring elements using interval coding. Pattern Recognition Letters. 1989;9(3):201-9. doi: 10.1016/0167-8655(89)90055-x. PubMed PMID: WOS:A1989U514000008.

13. Adams R, Bischof L. SEEDED REGION GROWING. Ieee Transactions on Pattern Analysis and Machine Intelligence. 1994;16(6):641-7. doi: 10.1109/34.295913. PubMed PMID: WOS:A1994NR97200008.

14. Nattkemper TW, Twellmann T, Ritter H, Schubert W. Human vs. machine: evaluation of fluorescence micrographs. Computers in Biology and Medicine. 2003;33(1):31-43. doi: 10.1016/s0010-4825(02)00060-4. PubMed PMID: WOS:000180493700003.

15. Tchoukalova YD, Harteneck DA, Karwoski RA, Tarara J, Jensen MD. A quick, reliable, and automated method for fat cell sizing. Journal of Lipid Research. 2003;44(9):1795-801. doi: 10.1194/jlr.D300001-JLR200. PubMed PMID: WOS:000185522300024.

16. Daims H, Lucker S, Wagner M. daime, a novel image analysis program for microbial ecology and biofilm research. Environmental Microbiology. 2006;8(2):200-13. doi: 10.1111/j.1462-2920.2005.00880.x. PubMed PMID: WOS:000234647600003.

17. Lempitsky V, Rother C, Roth S, Blake A. Fusion Moves for Markov Random Field Optimization. Ieee Transactions on Pattern Analysis and Machine Intelligence. 2010;32(8):1392-405. doi: 10.1109/tpami.2009.143. PubMed PMID: WOS:000278858600004.

18. Klinger-Strobel M, Suesse H, Fischer D, Pletz MW, Makarewicz O. A Novel Computerized Cell Count Algorithm for Biofilm Analysis. Plos One. 2016;11(5). doi: 10.1371/journal.pone.0154937. PubMed PMID: WOS:000375676800095.

19. Abramoff MD, Magalhães PJ, Ram SJ. Image processing with ImageJ2004; 11(7):[36-42 pp.].

20. Selinummi J, Seppala J, Yli-Harja O, Puhakka JA. Software for quantification of labeled bacteria from digital microscope images by automated image analysis. Biotechniques. 2005;39(6):859-63. doi: 10.2144/000112018. PubMed PMID: WOS:000234104900011.

21. Kayumov AR, Nureeva AA, Trizna EY, Gazizova GR, Bogachev MI, Shtyrlin NV, et al. New

552 Derivatives of Pyridoxine Exhibit High Antibacterial Activity against Biofilm-Embedded
553 Staphylococcus Cells. Biomed Research International. 2015:10. doi: 10.1155/2015/890968. PubMed
554 PMID: WOS:000367944100001.
555 22. Trizna E, Latypova L, Kurbangalieva A, Bogachev MI, Kayumov A. 2(5H)-Furanone
556 Derivatives as Inhibitors of Staphylococcal Biofilms. Bionanoscience. 2016;6(4):423-6. doi:
557 10.1007/s12668-016-0258-1. PubMed PMID: WOS:000390587700036.
558 23. Trizna EY, Khakimullina EN, Latypova LZ, Kurbangalieva AR, Sharafutdinov IS, Evtyugin
559 VG, et al. Thio Derivatives of 2(5H)-Furanone As Inhibitors against Bacillus subtilis Biofilms. Acta
560 Naturae. 2015;7(2):102-7. PubMed PMID: WOS:000355757100013.
561 24. Baidamshina DR, Trizna EY, Holyavka MG, Bogachev MI, Artyukhov VG, Akhatova FS, et al.
562 Targeting microbial biofilms using Ficin, a nonspecific plant protease. Scientific Reports. 2017;7. doi:
563 10.1038/srep46068. PubMed PMID: WOS:000398641900002.
564
565
566